Environmental Pollution 159 (2011) 3468–3473

Contents lists available at SciVerse ScienceDirect

Environmental Pollution

journal homepage: www.elsevier.com/locate/envpol

The effect of γ-Fe_2O_3 nanoparticles on *Escherichia coli* genome

Shiying He [a,1], Youzhi Feng [b,1], Ning Gu [a,*], Yu Zhang [a], Xiangui Lin [b]

[a] Jiangsu Laboratory for Biomaterials and Devices, School of Biological Science and Medical Engineering, Southeast University, Sipailou 2#, Nanjing 210096, PR China
[b] State Key Laboratory of Soil and Sustainable Agriculture, Institute of Soil Science, Chinese Academy of Sciences, Nanjing 210008, PR China

ARTICLE INFO

Article history:
Received 27 April 2011
Received in revised form
30 July 2011
Accepted 11 August 2011

Keywords:
Mutations
Escherichia coli
γ-Fe_2O_3 nanoparticles

ABSTRACT

Extensive production and application of γ-Fe_2O_3 magnetic nanoparticles (MNPs) has increased their potential risk on environment and human health. This report illustrates a genetic impact of γ-Fe_2O_3 magnetic nanoparticles (MNPs) on *Escherichia coli* (*E. coli*). After 3000-generation incubation with MNPs addition, obvious genomic variations were revealed by using repetitive extragenic palindromic PCR (rep-PCR) DNA fingerprint technique. The physicochemical interactions between MNPs and bacteria could be responsible for such genomic responses. It was revealed that Fe^{3+} concentration increased in the medium. Transmission electronic microscopy (TEM) and flow cytometry (FCM) analysis consistently demonstrated the occurrences of adsorption and membranes-internalization of MNPs outside and inside cells. Both increased Fe^{3+} ion and the uptake of MNPs facilitated Fe binding with proteins and DNA strands, resulting in enhancing the mutation frequency of *E. coli*. Our results would be of great help to assessing the potential impact of MNPs on human and environment.

1. Introduction

The iron oxide magnetic nanoparticles (MNPs) are one of the most widely studied nanomaterials. Due to their novel properties, such as enhanced surface-to-volume ratio, superparamagnetism and inherent biocompatibility (Perez et al., 2002; Sjogren et al., 1997), MNPs are being widely used for various biomedical and environmental applications such as magnetic resonance imaging (MRI), targeted delivery of drugs, targeted destruction of tumor tissue, magnetic bioseparations and pollution remediation etc (Kawashita et al., 2005; Prashant et al., 2010; Song et al., 2006; Telling et al., 2009; Veiseh et al., 2005; Wang and Irudayaraj, 2010). With continually increased applications, the exposure of such nanoparticles to human and environment is inevitable through the intentional releases as well as the unintentional discharges from production facilities at the end of their life circles (Lee et al., 2010). The exposure ultimately affects the health of ecosystem and human population. Although the potential benefits of MNPs are fully considerable, there is a distinct need to identify any potential negative responses of ecosystem and human. Unfortunately, the safety of MNPs is not clearly elucidated yet. Most investigations are focused on studying effects of MNPs on cellular viability, morphology and metabolism (Auffan et al., 2008; Xia et al., 2006). We reasoned that these physiological changes are indeed extrinsic exhibitions of genomic mutations induced by nanoparticles. However, thorough studies about their long-term impact on genomes are very limited.

Herein, we examined *Escherichia coli* (*E. coli*) genomic responses to γ-Fe_2O_3 MNPs at the molecular level by repetitive extragenic palindromic PCR (rep-PCR). The rep-PCR DNA fingerprinting technique has proven to be a valuable tool to identify, track and examine genotypic diversity among medically and environmentally important microorganisms (Ishii and Sadowsky, 2009). It is a simple and rapid method that has the necessary resolving power for microbial identification at subspecies or strain level. *E. coli*, a Gram negative rod-shaped bacterium, is one of the best-studied prokaryotic model organisms. It is commonly found in the environment and lower intestine of human. Most *E. coli* strains do not cause disease under normal circumstances but participate in maintaining human health, however, certain strains of *E. coli* mutated can produce potentially lethal toxins. Although, the interaction of metal oxide nanoparticles with bacteria has already been demonstrated (Auffan et al., 2008; Brayner et al., 2006; Dehner et al., 2011; Kasemets et al., 2009; Pelletier et al., 2010; Stoimenov et al., 2002), very few studies have been done to assess the mutagenic potential impact of nanoparticles on bacteria. Thus, it is important and urgent to study the effect of MNPs on *E. coli* genome, because genetic changes in *E. coli* may eventually induce some negative impacts on environment and human health. The impact of bulk (micro-scale) iron oxide particles was also assessed for comparative purposes.

* Corresponding author.
E-mail address: guning@seu.edu.cn (N. Gu).
[1] The first two authors have the equivalent contribution to the manuscript.

0269-7491/$ – see front matter © 2011 Elsevier Ltd. All rights reserved.
doi:10.1016/j.envpol.2011.08.024

2. Materials and methods

2.1. Chemicals and materials

$FeCl_3 \cdot 6H_2O$, $FeSO_4 \cdot 7H_2O$ and $(CH_3)_4NOH$ were obtained from Chemical Reagents Research Institute (Shanghai, China). Meso-2, 3-dimercaptosuccinic acid (DMSA) was from Sigma. Bacterial DNA kit was from Omega. DNA polymerase was from TaKaRa. Other reagents and chemicals were at least analytical reagent grade. Micro-sized iron oxide particles were purchased from Shanghai Demo Chemical Technology Co., China. Standard strain of *E. coli* (ATCC 25922) was from China General Microbiological Culture Collection Center.

2.2. Synthesis of γ-Fe_2O_3 MNPs

Iron oxide nanoparticles were synthesized by chemical coprecipitation of Molday. Typically, a solution of $FeCl_3$ and $FeSO_4$ mixture (molar ratio 2:1) was prepared under N_2 protecting, followed by the slow addition of enough ammonia aqueous solution with vigorous stirring for 30 min. The black Fe_3O_4 precipitates were obtained and washed immediately with distilled water for five times by magnetic separation. The final precipitates were dispersed in distilled water with concentration of 0.128 M and pH 3.0, and oxidized into more stable γ-Fe_2O_3 by air at the temperature of 90 °C. During this step, the initial black slurry turning into brown could be observed. The prepared γ-Fe_2O_3 nanoparticles were dispersed in deionized water, and the pH of the solution was adjusted to 2.7. Then, DMSA dissolved in DMSO was added to the dispersion with continuous stirring. After the reaction for 5 h at room temperature, the products were collected with a magnet and were dispersed in $(CH_3)_4NOH$ solution, and the pH of the solution was adjusted to 10. The stable magnetic fluids were obtained after the pH of the solution was adjusted to neutral. Coated nanoparticles were washed for five times with distilled water by magnetic separation to remove chemical residues. Then MNPs were resuspended in distilled water and sterilized through a 0.22 μm sterilized filter and stored at 4 °C for use.

2.3. Bacteria strain and incubation with particles

E. coli strain ATCC 25922 was used as test microorganism in this study. The bacteria were grown aerobically in a vial at 37 °C with shaking (200 rpm) in Luria-Bertani nutrient medium (LB) (5 g L^{-1} NaCl, 10 g L^{-1} tryptone powder, and 5 g L^{-1} beef extract powder, pH 7.2). The γ-Fe_2O_3 nanoparticles were administered in the LB nutrient medium achieving an exposure concentration of 0.1 mg/ml (Chen et al., 2011; Gu et al., 2009). *E. coli* was subcultured every 12–16 h until 3000 generations after 40-day incubation in liquid medium with/without MNPs at 37 °C with shaking (200 rpm). Then 100 μl bacterial suspensions amended with MNPs or not were inoculated on LB agar and grown at 37 °C. Colonies appeared on medium plates after 16 h of incubation. Sixteen colonies were randomly selected and suspended in 100 μl of sterile distilled water for rep-PCR analysis. Bulk particles of the iron oxide (1–3 μm, Fig. S1) were also used to assess their impact on *E. coli* genome as comparison.

2.4. DNA extraction and rep-PCR amplification

Genomic DNA was subsequently extracted using bacterial DNA kit (Omega), following the specifications of the manufacturer. The extracted DNA was eluted and stored at −80 °C until it was analyzed. Equal amount of DNA samples (ca. 20 ng/μl) were subjected to rep-PCR amplification using primer BOX A1R (5′-CTACGG CAAGGCGACGCTGACG-39′). PCR were carried out in 25-μl reaction mixtures containing Gitschier buffer [83 mM $(NH4)_2SO_4$, 335 mM Tris–HCl (pH 8.8), 33.5 mM $MgCl_2$, 33.5 mM EDTA, 150 mM β-mercaptoethanol], 4 μg of bovine serum albumin per ml, 10% (vol/vol) dimethyl sulfoxide, each deoxynucleoside triphosphate at a concentration of 1.25 mM, 2 μM BOX A1R primer, 2 U of *Taq* DNA polymerase (TaKaRa, Japan), and 50 ng of DNA. The temperature profile was as follows: initial denaturation at 95 °C for 2 min; 35 cycles of 94 °C for 3 s, 92 °C for 30 s, 50 °C for 1 min, and 65 °C for 8 min; and final extension at 65 °C for 8 min. PCR products were separated by electrophoresis on 1.5% agarose gels at 70 V and 4 °C for 19 h. After the agarose gels were stained with ethidium bromide, images of the gels were digitized by using a Gel Doc™ EQ imager combined with Quantity one 4.4.0 (Bio-Rad). Cluster analysis of similarity matrices was performed by an unweighted pair group using mathematical averages (UPGMA).

2.5. Iron ion concentration measurement in suspension

The solubility of MNPs in the LB medium was quantified. The particles suspension was centrifuged at 10,000 g for 10 min. The supernatant was carefully collected and filtered through 0.22 μm filter. The ion concentration was measured via an inductively coupled plasma optical emission spectrometer (ICP-OES).

2.6. Characterization of MNPs

The size and morphology of MNPs were determined by transmission electronic microscopy (TEM) (JEOL/JEM-2000E). 5 μl of the MNPs solution was placed onto the carbon-coated copper grids and allowing the solvent to evaporate in the air. MNPs diameter distribution was determined with image software by analyzing more than 400 particles. Zeta potential (ζ) of MNPs in LB medium was performed with a zeta potential analyzer (BECKMAN, Delsa 440SX).

2.7. Ultrathin section electron microscopy measurement

Characterization of the interaction of MNPs with bacteria was also done. Thin sections of samples embedded in a resin were prepared for TEM measurement. Control and MNP-treated bacterial samples were fixed for 3 h with 2.5% glutaraldehyde in 0.1 M cacodylate buffer (pH 7.4). After washing with cacodylate buffer, they were further fixed with 1% osmic acid for 2 h and washed with PBS for three times. The cells were then dehydrated through graded ethanol solutions with 30, 50, 70, 90, 95, 100% (v/v, in water), and 50% ethanol in acetone for 10 min each time. The samples were finally dehydrated with pure acetone twice for 15 min. Ultrathin sections of 60–80 nm were cut using an ultramicrotome and mounted on a carbon-coated copper TEM grid. The sections were stained with 2% uranyl acetate in distilled water for 10 min and lead staining solution for 5 min prior to TEM analysis. The surface morphologies of *E. coli* and MNPs-treated *E. coli* were by scanning electron microscopy (SEM, JEOL, JSM-5610LV).

2.8. Detection of nanoparticles uptake through flow cytometry

Flow cytometry (FCM) was also performed for analyzing the uptake of MNPs in the cells. Generally, it is considered that the side scatter (SSC) provides information on internal structures and organelles and the forward scatter (FSC) reflects the size of a cell. We demonstrated here the effects that MNPs interacting with cells on SSC and FSC signal obtained by flow cytometry at 488 nm argon-ion laser (BD FACSCalibur, BD Biosciences, San Jose, CA, USA). For FCM detection, cells were thoroughly washed with PBS to remove nanoparticles, harvested and prepared into single cell suspension, and then loaded to flow cytometry. At least 10^5 cells were tested for each sample. For data analysis, the value of SSC intensity was divided into four regions: M1 (0–200), M2 (200–400), M3 (400–600), and M4 (600–1000). Data were analyzed using CellQuest™ software.

2.9. Toxicity assessment

The experiments were designed to check whether the MNPs are able to alter cell growth. The concentration of *E. coli* grown with and without MNPs after incubation for a certain time was determined using UV–vis spectroscopy at 600 nm.

Each treatment was conducted with three replicates, and the results were presented as mean SD (standard deviation). The statistical analysis of experimental data utilized the Student's *t*-test. Each of the experimental values was compared to its corresponding control. Statistical significance was accepted when the probability of the result assuming the null hypothesis (p) is less than 0.05.

3. Results and discussion

3.1. MNPs induced changes of E. coli genotypes

Fig. 1a shows a representative TEM of the MNPs generated by coprecipitation. The particles were quasi-spherical in shape. The statistical analysis of MNPs diameters indicates the size distribution of particles and that the main were around 10 nm (Fig. 1b). It was also shown that nanoparticles modified by DMSA via surface double-exchange kept well dispersed with a little aggregation in LB medium (Fig. 1a). The underlying mechanism is due to the negative value ζ of around −52 mV, which makes particles repel each other. Such well-dispersed MNPs can keep stable in aqueous solution at 4 °C at least for one year. The effect of MNPs on *E. coli* genotypes at a molecular level was investigated by rep-PCR genomic DNA fingerprinting. Typical images of results of rep-PCR can be seen in Fig. 2. It is considered that genotypes having relative similarity values greater than 80% are representatives of a single strain (Oda et al., 2002). Based on this criterion, several different genotypes of *E. coli*, which are marked by different colors respectively, were observed when treated with MNPs. rep-PCR fingerprinting patterns of the *in vitro* amplification of DNA extracted from cells treated with MNPs formed different clusters in the dendrogram (Fig. 2). Only 6% of MNPs-treated *E. coli* strains shared 85% similarity with those in control (shown in point A). 50% of strains had about 70% similarity with those in control (shown in point B). Moreover, 18.7% had only 47% similarity with those in control (shown in point C). In contrast,

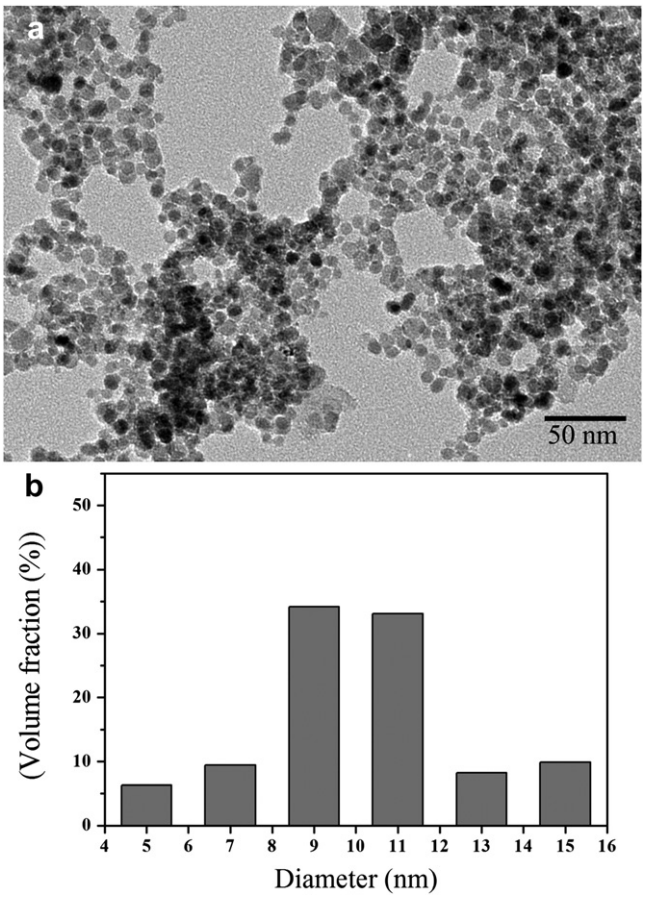

Fig. 1. a. TEM micrograph of γ-Fe_2O_3 nanoparticles; b. Relative size distribution of γ-Fe_2O_3 nanoparticles. The intensity scale on the *y*-axis represents the volume fraction of each size.

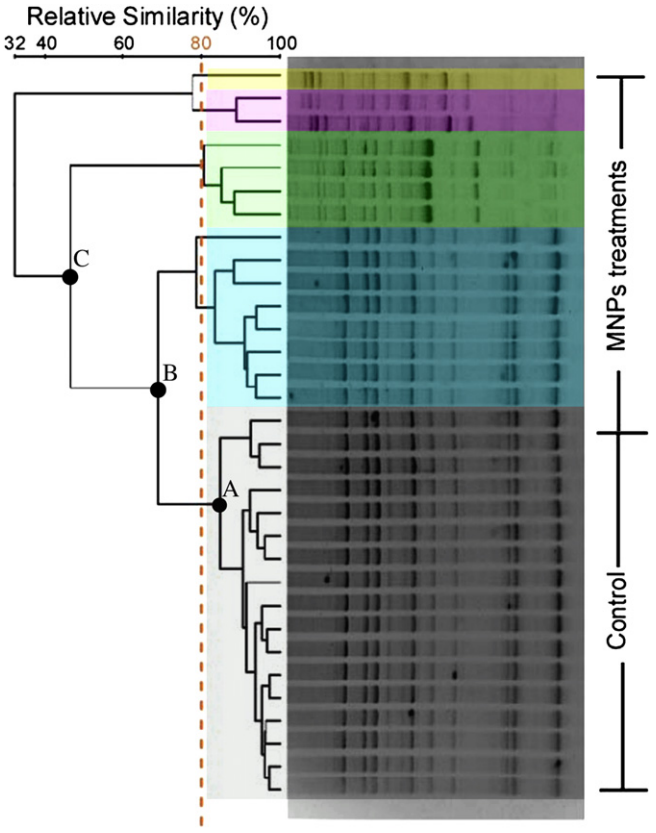

Fig. 2. Agarose gel electrophoresis of rep-PCR products. Dendrogram shows similarities of *E. coli* strains from control and MNPs treatments. Relationships between DNA fingerprints were determined by an unweighted pair group using mathematical averages (UPGMA).

the *in vitro* amplification of DNA extracted from cells under control showed the almost identical genomic fingerprinting patterns (>93%). The genotypes in bulk-Fe_2O_3 particles treatment had also no obvious difference (>84%, Fig. S2). Thus, the appearance of different genotypes in γ-Fe_2O_3 MNPs treatments indicates that MNPs induce mutations of *E. coli*.

3.2. Physicochemical interaction of MNPs with E. coli

Physicochemical interferences of MNPs on *E. coli* are suggested to be of the critical factors for bacterial mutations as shown in scheme (Fig. 3). Nano metal oxide particles have been found to be capable of penetrating cell wall and entering bacterial cells (Brayner et al., 2006; Dehner et al., 2011). Consistently, γ-Fe_2O_3 MNPs was found to adsorb and enter bacteria cell in this report. Subsequently the MNPs may interact with the cellular macromolecules such as protein and chromosome.

The uptake of MNPs by *E. coli* cells was demonstrated using FCM. SSC signal reflects the density and granularity of a cell, higher density and more granules with stronger SSC signal. It has been observed that SSC was increased upon cellular uptake of the nanoparticles in human cells using FCM (Zucker et al., 2010). In this study, after the incubation with MNPs, SSC intensity increased evidently as compared to the control (as shown in Fig. 4). The percentage of cells in the region of M1 (low signal intensity) decreased significantly, resulting in corresponding increase of cells in the regions of M2 and M3 (high signal intensity). For cells incubated with MNPs, the mean intensity of SSC was 306, showing significant increase compared to 186 of control cells. The forward scatter (FSC) reflects the size of a cell. The mean intensity of FSC almost did not change compared with control cells, showing that cells could keep their sizes during the absorption of nanoparticles (histograms not shown).

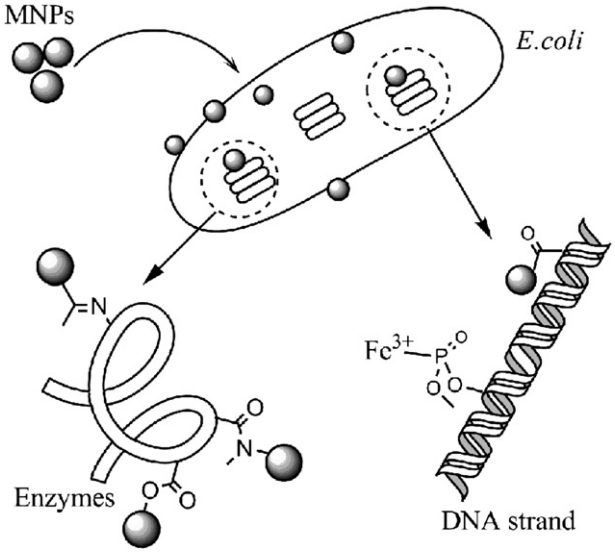

Fig. 3. Schematic illustration of the possible mechanisms of MNPs interacting with bacteria.

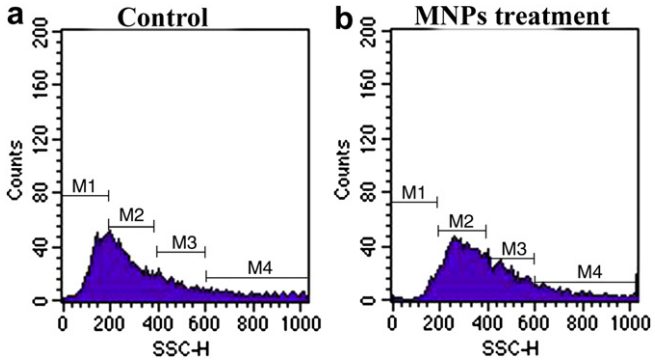

Fig. 4. Side scatter signal of *E. coli* cells detected by flow cytometry (488 nm Argon laser). (a) Control cells, (b) cells incubation with γ-Fe_2O_3 MNPs.

SEM and TEM were used to directly visualize locations of MNPs and changes in cell morphology. Fig. 5a and b show SEM images of cells in LB medium with and without MNPs. Normally, morphologies of cells are of bacilliform shape with a moderate size (1.5 μm × 0.5 μm). When exposed to MNPs, the sizes of cells were similar to those in control, which is consistent with the results of FSC. However, a layer of MNPs are observed to be absorbed at membranes of cell wall. The possible mechanism would be due to bacterial wall constitution. Carboxyl, amide, phosphate, hydroxyl groups and carbohydrate-related moieties in bacterial cell wall may provide sites for binding with MNPs (Lovern et al., 2007; Omoike and Chorover, 2004).

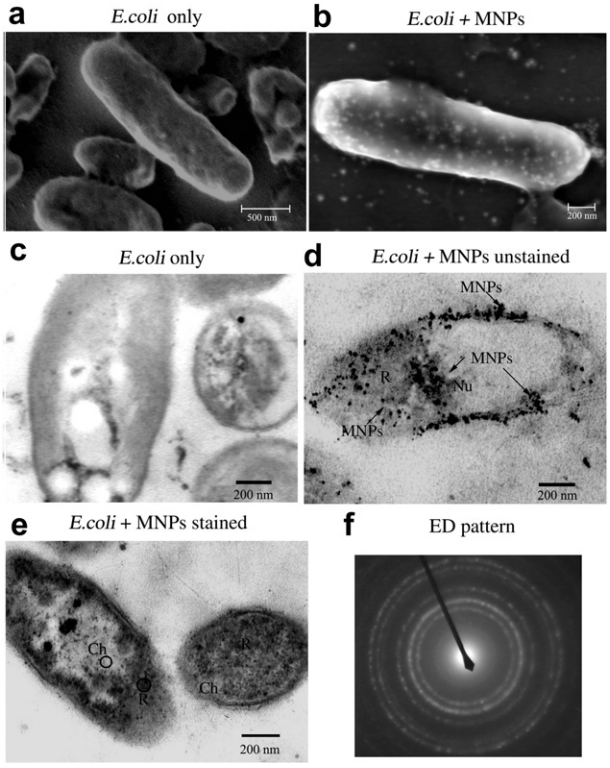

Fig. 5. Location of γ-Fe_2O_3 MNPs in *E. coli*. a, b: SEM of bacteria cultivated in LB medium without and with MNPs; c, d: TEM of superthin slices of *E. coli* cultivated in LB medium without and with MNPs. e: TEM of stained superthin slices of *E. coli* indicates that MNPs bind to ribosomes and chromosomes. f: ED analysis of the area enclosed with a black circle. In Fig. 3d and e, Nu = nuclear material, R = ribosome, Ch = chromosome.

TEM revealed that MNPs located not only at cell wall and outer membrane, but also at cytoplasm membrane and in cytoplasm (Fig. 5d). The cytoplasm shows unanimous electron density when without MNPs (Fig. 5c). In the presence of MNPs, the cytoplasm of *E. coli* clearly displays an uneven electronic density (Fig. 5d), which might be attributed to the internalization of MNPs. It is well known that prokaryotic cells utilize membrane anchored protein channels for uptakes of large molecules (Schulz, 2002). Molecules with a maximum size range 1.8–2 nm are allowed for non-specific uptake in gram-negative cells (Trias and Benz, 1994). Therefore the possible reason for the entry of nanoparticles (average 10 nm) into a bacterial cell is due to damages of cell wall. As shown in Fig. 5d, several sites of cell membranes in *E. coli* are damaged, which could lead to the entry and internalization of MNPs.

Cytoplasm is filled with ribosome and nuclear material. The entering of nanoparticles facilitates their binding with proteins and DNA strands. TEM graphs of superthin slices stained with uranyl acetate and lead citrate can clearly discern bindings of MNPs to ribosome and chromosomes (Fig. 5e and f). Electron-dense area indicates ribosome, while electron-light region indicates nuclear material (Someya et al., 1979; Zhao et al., 2010). The binding of MNPs and ribosome as well as chromosomes would subsequently affect conformations of DNA strands and proteins. As shown in scheme, γ-Fe_2O_3 nanoparticles interact with DNA assembling as a nanocomposite (Dutta et al., 2006). Formation of DNA-γ-Fe_2O_3 nanocomposite affects gene semi-conservative replication. The four bases, adenine, guanine, thymine, and cytosine (A, G, T, and C), contain carbonyl groups that display high affinities to nanoparticles (Kouassi and Irudayaraj, 2006). As a result, bacterial DNA conformation could be transformed. Similarly, nanoparticles have high affinity with proteins (Dyal et al., 2003). Enzymes involved in DNA replication, hence, could bind MNPs, such as helicases, DNA ligase, DNA synthase etc. Both above processes would raise DNA mismatch during semi-conservative replication, further increase the mutation frequency and finally produce mutants of *E. coli*.

Another crucial factor which may affect *E. coli* is the release of metal ions from nanoparticles. It has been shown previously that the toxicity of nano-ZnO is directly related to particle dissolution and release of toxic Zn^{2+} in the cell culture medium as well as the uptake of the particle remnants in the cells (Nel et al., 2008). We studied the dissolution of iron oxide nanoparticles in LB medium. Using ICP-OES, the maximal dissolved Fe^{3+} of nanoparticles in LB medium was 18.3 μg/ml (Fig. 6). As a result, the dissolved Fe^{3+} might enter the cytoplasm. Fe^{3+} cation shows stronger interaction

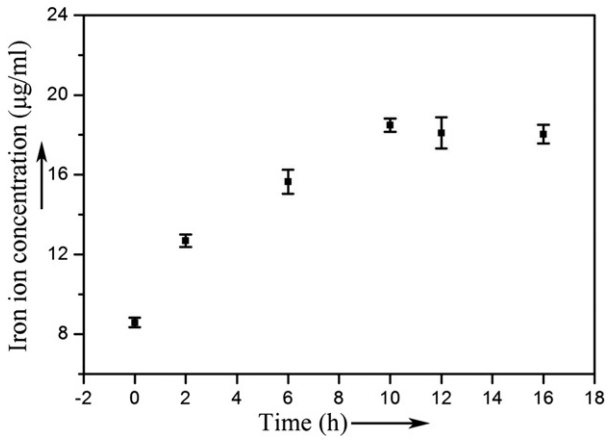

Fig. 6. The dissolution of Fe^{3+} ions in LB medium during *E. coli* cultivation. Each data point is the average of three replicates, with error bars denoting the standard deviation.

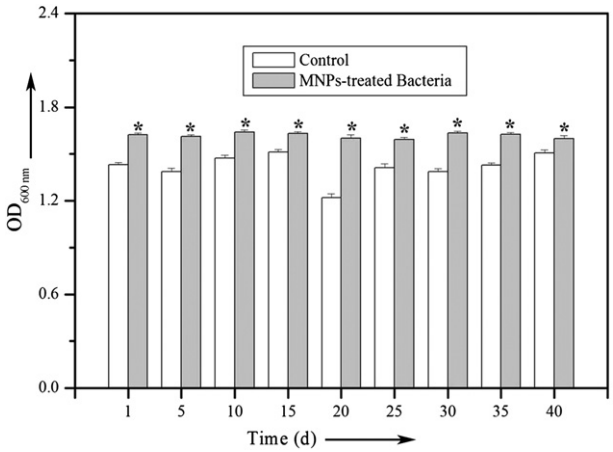

Fig. 7. Optical densities at 600 nm ($OD_{600\ nm}$) of bacterial suspension treated with and without MNPs. Data are means of three determinations and the error bars indicate standard deviation. Values are representative of three independent experiments. *Significant difference to control ($P < 0.05$).

with bases and backbone phosphate groups of DNA (Ouameur et al., 2005). This process is prone to make DNA mutation during replication.

3.3. Cytotoxicity of MNPs

Surprisingly, MNPs amendment didn't inhibit growths of *E. coli* strains when measured following the protocol described in the cytotoxicity assays section. By contrast, cell densities were even higher in MNPs treatments than in control (Fig. 7), indicating that bacterial growth is indeed promoted by MNPs. The underlying mechanism could be that the presence of iron in environments can facilitate both growth and cultivability of *E. coli*, because iron can serve as both a nutrient and an electron acceptor (Appenzeller et al., 2005).

Overall, our work showed that *E. coli* cells suffered genomic mutations under MNPs treatments. Both increased Fe^{3+} ion and the uptake of MNPs facilitated Fe binding with proteins and DNA strands, resulting in enhancing the mutation frequency of *E. coli*. The results also showed that MNPs might promote bacterial growth by offering iron element. Future work is necessary to apply pyro-sequencing approach to elucidate variation in genome of *E. coli* in detail and to combine its genotype and phenotype to deeply figure out the characteristics of mutants of *E. coli* under MNPs treatment.

Acknowledgments

This work was financially supported by National Natural Science Foundation of China (Project: 41001142, 60501009) and China-US International Science and Technology Cooperation Program (2009DFA31990).

Appendix. Supplementary material

Supplementary material associated with this article can be found, in the online version, at doi:10.1016/j.envpol.2011.08.024.

References

Appenzeller, B.M.R., Yanez, C., Jorand, F., Block, J.C., 2005. Advantage provided by iron for *Escherichia coli* growth and cultivability in drinking water. Applied and Environmental Microbiology 71, 5621–5623.

Auffan, M., Achouak, W., Rose, J., Roncato, M.A., Chaneac, C., Waite, D.T., Masion, A., Woicik, J.C., Wiesner, M.R., Bottero, J.Y., 2008. Relation between the redox state of iron-based nanoparticles and their cytotoxicity toward *Escherichia coli*. Environmental Science & Technology 42, 6730–6735.

Brayner, R., Ferrari-Iliou, R., Brivois, N., Djediat, S., Benedetti, M.F., Fievet, F., 2006. Toxicological impact studies based on *Escherichia coli* bacteria in ultrafine ZnO nanoparticles colloidal medium. Nano Letters 6, 866–870.

Chen, Y.S., Zhang, W., Rittmann, B., 2011. Size effects on adsorption of hematite nanoparticles on *E. coli* cells. Environmental Science & Technology 45, 2172–2178.

Dehner, C.A., Barton, L., Maurice, P.A., Dubois, J.L., 2011. Size-dependent bioavailability of hematite (alpha-Fe_2O_3) nanoparticles to a common aerobic bacterium. Environmental Science & Technology 45, 977–983.

Dutta, P., Manivannan, A., Seehra, M.S., Shah, N., Huffman, G.P., 2006. Magnetic and structural properties of a DNA-maghemite nanocomposite. Journal of Applied Physics 99, 105–107.

Dyal, A., Loos, K., Noto, M., Chang, S.W., Spagnoli, C., Shafi, K.V.P.M., Ulman, A., Cowman, M., Gross, R.A., 2003. Activity of *Candida rugosa* lipase immobilized on gamma-Fe_2O_3 magnetic nanoparticles. Journal of the American Chemical Society 125, 1684–1685.

Gu, N., Zhang, S., Chen, X.J., Gu, C.R., Zhang, Y., Xu, J.D., Bian, Z.P., Yang, D., 2009. The effect of iron oxide magnetic nanoparticles on smooth muscle cells. Nanoscale Research Letters 4, 70–77.

Ishii, S., Sadowsky, M.J., 2009. Applications of the rep-PCR DNA fingerprinting technique to study microbial diversity, ecology and evolution. Environmental Microbiology 11, 733–740.

Kasemets, K., Ivask, A., Dubourguier, H.C., Kahru, A., 2009. Toxicity of nanoparticles of ZnO, CuO and TiO_2 to yeast *Saccharomyces cerevisiae*. Toxicology in Vitro 23, 1116–1122.

Kawashita, M., Tanaka, M., Kokubo, T., Inoue, Y., Yao, T., Hamada, S., Shinjo, T., 2005. Preparation of ferrimagnetic magnetite microspheres for in situ hyperthermic treatment of cancer. Biomaterials 26, 2231–2238.

Kouassi, G.K., Irudayaraj, J., 2006. Magnetic and gold-coated magnetic nanoparticles as a DNA sensor. Analytical Chemistry 78, 3234–3241.

Lee, J., Mahendra, S., Alvarez, P.J.J., 2010. Nanomaterials in the construction industry: a review of their applications and environmental health and safety considerations. Acs Nano 4, 3580–3590.

Lovern, S.B., Strickler, J.R., Klaper, R., 2007. Behavioral and physiological changes in *Daphnia magna* when exposed to nanoparticle suspensions (titanium dioxide, nano-C-60, and C(60)HxC(70)Hx). Environmental Science & Technology 41, 4465–4470.

Nel, A.E., Xia, T., Kovochich, M., Liong, M., Madler, L., Gilbert, B., Shi, H.B., Yeh, J.I., Zink, J.I., 2008. Comparison of the mechanism of toxicity of zinc oxide and cerium oxide nanoparticles based on dissolution and oxidative stress properties. Acs Nano 2, 2121–2134.

Oda, Y., Wanders, W., Huisman, L.A., Meijer, W.G., Gottschal, J.C., Forney, L.J., 2002. Genotypic and phenotypic diversity within species of purple nonsulfur bacteria isolated from aquatic sediments. Applied and Environmental Microbiology 68, 3467–3477.

Omoike, A., Chorover, J., 2004. Spectroscopic study of extracellular polymeric substances from *Bacillus subtilis*: aqueous chemistry and adsorption effects. Biomacromolecules 5, 1219–1230.

Ouameur, A.A., Arakawa, H., Ahmad, R., Naoui, M., Tajmir-Riahi, H.A., 2005. A comparative study of Fe(II) and Fe(III) interactions with DNA duplex: major and minor grooves bindings. DNA and Cell Biology 24, 394–401.

Pelletier, D.A., Suresh, A.K., Holton, G.A., McKeown, C.K., Wang, W., Gu, B.H., Mortensen, N.P., Allison, D.P., Joy, D.C., Allison, M.R., Brown, S.D., Phelps, T.J., Doktycz, M.J., 2010. Effects of engineered cerium oxide nanoparticles on bacterial growth and viability. Applied and Environmental Microbiology 76, 7981–7989.

Perez, J.M., O'Loughin, T., Simeone, F.J., Weissleder, R., Josephson, L., 2002. DNA-based magnetic nanoparticle assembly acts as a magnetic relaxation nanoswitch allowing screening of DNA-cleaving agents. Journal of the American Chemical Society 124, 2856–2857.

Prashant, C., Dipak, M., Yang, C.T., Chuang, K.H., Jun, D., Feng, S.S., 2010. Superparamagnetic iron oxide - loaded poly (lactic acid)-D-alpha-tocopherol polyethylene glycol 1000 succinate copolymer nanoparticles as MRI contrast agent. Biomaterials 31, 5588–5597.

Schulz, G.E., 2002. The structure of bacterial outer membrane proteins. Biochimica Et Biophysica Acta-Biomembranes 1565, 308–317.

Sjogren, C.E., Johansson, C., Naevestad, A., Sontum, P.C., BrileySaebo, K., Fahlvik, A.K., 1997. Crystal size and properties of superparamagnetic iron oxide (SPIO) particles. Magnetic Resonance Imaging 15, 55–67.

Someya, A., Tanaka, K., Tanaka, N., 1979. Morphological-changes of *Escherichia coli* induced by bicyclomycin. Antimicrobial Agents and Chemotherapy 16, 87–91.

Song, M., Zhang, R.Y., Dai, Y.Y., Gao, F., Chi, H.M., Lv, G., Chen, B.A., Wang, X.M., 2006. The in vitro inhibition of multidrug resistance by combined nanoparticulate titanium dioxide and UV irradiation. Biomaterials 27, 4230–4238.

Stoimenov, P.K., Klinger, R.L., Marchin, G.L., Klabunde, K.J., 2002. Metal oxide nanoparticles as bactericidal agents. Langmuir 18, 6679–6686.

Telling, N.D., Coker, V.S., Cutting, R.S., van der Laan, G., Pearce, C.I., Pattrick, R.A.D., Arenholz, E., Lloyd, J.R., 2009. Remediation of Cr(VI) by biogenic magnetic nanoparticles: an x-ray magnetic circular dichroism study. Applied Physics Letters 95, 163701–163703.

Trias, J., Benz, R., 1994. Permeability of the cell-wall of *Mycobacterium smegmatis*. Molecular Microbiology 14, 283–290.

Veiseh, O., Sun, C., Gunn, J., Kohler, N., Gabikian, P., Lee, D., Bhattarai, N., Ellenbogen, R., Sze, R., Hallahan, A., Olson, J., Zhang, M.Q., 2005. Optical and MRI multifunctional nanoprobe for targeting gliomas. Nano Letters 5, 1003–1008.

Wang, C.G., Irudayaraj, J., 2010. Multifunctional magnetic-optical nanoparticle probes for simultaneous detection, separation, and thermal ablation of multiple pathogens. Small 6, 283–289.

Xia, T., Kovochich, M., Brant, J., Hotze, M., Sempf, J., Oberley, T., Sioutas, C., Yeh, J.I., Wiesner, M.R., Nel, A.E., 2006. Comparison of the abilities of ambient and manufactured nanoparticles to induce cellular toxicity according to an oxidative stress paradigm. Nano Letters 6, 1794–1807.

Zhao, Y.Y., Tian, Y., Cui, Y., Liu, W.W., Ma, W.S., Jiang, X.Y., 2010. Small molecule-capped gold nanoparticles as potent antibacterial agents that target gram-negative bacteria. Journal of the American Chemical Society 132, 12349–12356.

Zucker, R.M., Massaro, E.J., Sanders, K.M., Degn, L.L., Boyes, W.K., 2010. Detection of TiO(2) nanoparticles in cells by flow cytometry. Cytometry Part A 77A, 677–685.